

Copy

RM A55H09

15115
22
36

57-34-86

PLEASE RETURN TO
HOLLAND AIR FORCE BASE
ALABAMA

0143575



12 OCT 1955

NACA RM A55H09

3979

NACA

RESEARCH MEMORANDUM

EFFECTS OF BOUNDARY-LAYER SEPARATION ON NORMAL FORCE
AND CENTER OF PRESSURE OF A CONE-CYLINDER MODEL
WITH A LARGE BASE FLARE AT MACH NUMBERS
FROM 3.00 TO 6.28

By David H. Dennis and Clarence A. Syvertson

Ames Aeronautical Laboratory
Moffett Field, Calif.

Classification cancelled (or changed to.....)

By authority of..... (OFFICER AUTHORIZED TO CHANGE)

By
NAME AND

.....
GRADE OF OFFICER MAKING CHANGE)

CLASSIFIED DOCUMENT

..... This material contains information affecting the National Defense of the United States within the meaning of the espionage laws, Title 18, U.S.C., Secs. 793 and 794, the transmission or revelation of which in any manner to an unauthorized person is prohibited by law.

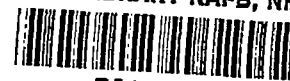
TECHNICAL LIBRARY
AFL 2291

NATIONAL ADVISORY COMMITTEE FOR AERONAUTICS

WASHINGTON
October 3, 1955

~~CONFIDENTIAL~~

NADC 55-4761



NATIONAL ADVISORY COMMITTEE FOR AERONAUTICS

RESEARCH MEMORANDUM

EFFECTS OF BOUNDARY-LAYER SEPARATION ON NORMAL FORCE

AND CENTER OF PRESSURE OF A CONE-CYLINDER MODEL

WITH A LARGE BASE FLARE AT MACH NUMBERS

FROM 3.00 TO 6.28

By David H. Dennis and Clarence A. Syvertson

SUMMARY

Results are presented of tests on a body having a $22\text{-}1/2^\circ$ conical nose, a 4-diameter-long cylindrical midsection and a 20° cone-frustum tail flare. The tests were made at small angles of attack over a Mach number range from 3.00 to 6.28. The corresponding Reynolds numbers based on body length ranged from 5.5 million to 1.0 million. The purpose of these tests was to determine how flow separation ahead of the tail flare can affect normal force and center of pressure.

Experiment revealed that flow separation increased markedly with simultaneously increasing Mach number and decreasing Reynolds number. As a result of separation, normal-force coefficient and center of pressure varied in an extremely nonlinear manner with angle of attack. Moreover, initial normal-force-curve slope increased by almost threefold with increasing Mach number and decreasing Reynolds number, and center of pressure moved aft close to the base of the body. Attempts to predict these large changes by conventional means were unsuccessful.

INTRODUCTION

Bodies with tail flares have recently attracted interest because of their stability in pitch and yaw in supersonic flight (see, e.g., ref. 1). Large flares have also been suggested for application to long-range ballistic vehicles to provide braking action during entry into the earth's atmosphere (ref. 2). It is known, however, that shock-wave boundary-layer interaction will tend to separate the flow from the junction of a flare with the main body of a vehicle (see ref. 1). It is important to inquire, then, how such separation affects the aerodynamic characteristics of a vehicle.

The purpose of the present paper is to report on a preliminary experimental investigation of the separation phenomenon as it relates to the normal-force and center-of-pressure characteristics on a body having a large base flare.

NOTATION

A	cylinder cross-section area
C_N	normal-force coefficient, $\frac{\text{normal force}}{qA}$
M	Mach number
q	free-stream dynamic pressure
R	free-stream Reynolds number based on body length
α	angle of attack

APPARATUS AND TESTS

The tests were conducted in the Ames 10- by 14-inch supersonic wind tunnel at Mach numbers of 3.00, 4.24, 5.05, and 6.28. For a detailed description of this wind tunnel and its flow characteristics see reference 3. Normal forces and pitching moments on the test model were determined with a strain-gage balance which consisted of a model support sting on which moments were measured at four points. From these four measurements, normal forces and centers of pressure were determined and checked. Measurements were made at angles of attack from -2° to $+4^\circ$.

Wind-tunnel calibration data (see ref. 3) were employed in combination with stagnation-pressure measurements to obtain stream static and dynamic pressures.

The model tested consisted of a conical nose section having a semi-apex angle of $22\frac{1}{2}^\circ$, followed by a 4-diameter-long cylinder, in turn followed by a cone frustum 2.4-cylinder-diameters long and having a cone semiangle of 20° . The diameter of the cylindrical section was 1 inch. A sketch of the model is shown in figure 1. Reynolds numbers based on the length (7.61 in.) of the model were:

<u>M</u>	<u>R, million</u>
3.00	5.5
4.24	4.8
5.05	2.6
6.28	1.0

The accuracy of the test results was influenced by uncertainties in the measurements of moments and stream dynamic pressure. These uncertainties resulted in estimated maximum errors in the values of normal-force coefficient and center of pressure of ± 0.02 and ± 2 percent of the body length, respectively. The uncertainty in angle-of-attack measurements was $\pm 0.05^\circ$. Stream Mach numbers in the region of the test body did not vary more than ± 0.03 from the mean values at Mach numbers up to 5.05. A maximum variation of ± 0.05 existed at the highest test Mach number of 6.28.

RESULTS AND DISCUSSION

Spark shadowgraph pictures of the air flow about the test body in the region of the cylinder-frustum juncture are presented in figure 2¹ to show the changes that occur in the extent of flow separation with increasing Mach number and decreasing Reynolds number. It may be seen in figures 2(a) and 2(b) that at $M = 3.00$ and 4.24 , $R = 5.5$ and 4.8 million, respectively, shock-wave boundary-layer interaction induces a relatively small region of separated flow. However, at $M = 5.05$, $R = 2.6$ million, and particularly at $M = 6.28$, $R = 1$ million, there are large separated-flow regions near the cylinder-frustum juncture (figs. 2(c) and 2(d)).

The corresponding changes that occur in the normal-force and center-of-pressure characteristics with increasing Mach number and decreasing Reynolds number are shown in figures 3 and 4. At Mach numbers of 3.00 and 4.24 (little flow separation), the variations of normal-force coefficient with angle of attack are very nearly linear (fig. 3) and the centers of pressure are virtually constant with changing angle of attack (fig. 4). At $M = 5.05$ and 6.28 (pronounced flow separation), the variations of normal-force coefficient with angle of attack are very nonlinear and the centers of pressure move forward appreciably with increasing angle of attack.

It also may be seen in figures 3 and 4 that with increasing Mach number and decreasing Reynolds number, the initial normal-force-curve slope increases markedly and the center of pressure at zero angle of attack moves aft to a position close to the body base. These characteristics

¹The horizontal dark streaks appearing in the pictures result from oil on the wind-tunnel windows and are not related to the flow about the model.

are shown more clearly in figure 5, where it may be seen that the initial normal-force-curve slope at the highest test Mach number is almost three times that at $M = 3.00$. Also shown in figure 5 are results of calculations made with the generalized shock-expansion method (ref. 4). The predictions of normal-force-curve slope and center-of-pressure position at $M = 3.00$ and 4.24 are good. However, at the higher Mach numbers where the separated-flow regions are extensive, the theoretical values are in large error.

Predictions of initial normal-force-curve slope and center-of-pressure position were also made considering the body shape to include that space enclosed by the separated-flow regions at $\alpha = 0^\circ$. The separated-flow regions were determined from the shadowgraph pictures. Agreement with the experimental results was not improved over the predictions shown in figure 5 for which separation effects were neglected. Evidently then, the large effects of separation on normal-force and center-of-pressure characteristics at the higher test Mach numbers cannot be predicted on the basis of the assumption that the body remains effectively axially symmetric at small angles of attack, and further experimental studies are required to understand these effects.

CONCLUSIONS

The results of tests at small angles of attack on a cone-cylinder cone-frustum model at Mach numbers from 3.00 to 6.28 and corresponding Reynolds numbers (based on body length) from 5.5 to 1.0 million have led to the following conclusions:

1. The extent of flow separation at the cylinder cone-frustum juncture increases appreciably with simultaneously increasing Mach number and decreasing Reynolds number.
2. For the test conditions where the extent of flow separation is large, the variations of normal-force coefficient and center of pressure with angle of attack are very nonlinear.
3. With increasing flow separation the initial normal-force-curve slope increases by approximately threefold and the center of pressure moves to a position very close to the body base.

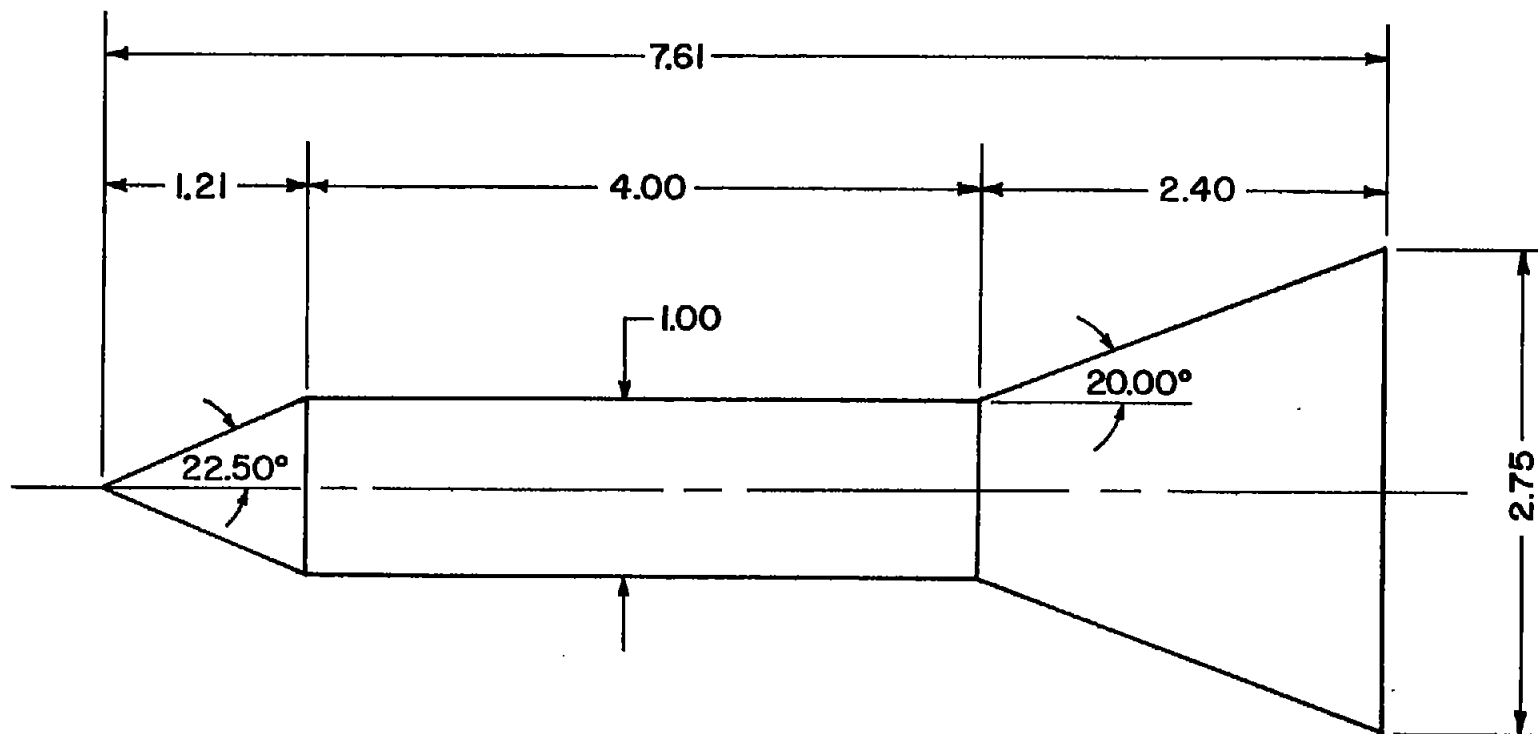
Ames Aeronautical Laboratory
National Advisory Committee for Aeronautics
Moffett Field, Calif., Aug. 9, 1955

REFERENCES

1. Eggers, A. J., Jr., and Syvertson, Clarence A.: Experimental Investigation of a Body Flare for Obtaining Pitch Stability and a Body Flap for Obtaining Pitch Control in Hypersonic Flight. NACA RM A54J13, 1955.
2. Allen, H. Julian, and Eggers, A. J., Jr.: A Study of the Motion and Aerodynamic Heating of Missiles Entering the Earth's Atmosphere at High Supersonic Speeds. NACA RM A53D28, 1953.
3. Eggers, A. J., Jr., and Nothwang, George J.: The Ames 10- by 14-Inch Supersonic Wind Tunnel. NACA TN 3095, 1954.
4. Savin, Raymond C.: Application of the Generalized Shock-Expansion Method to Inclined Bodies of Revolution Traveling at High Supersonic Airspeeds. NACA TN 3349, 1955.

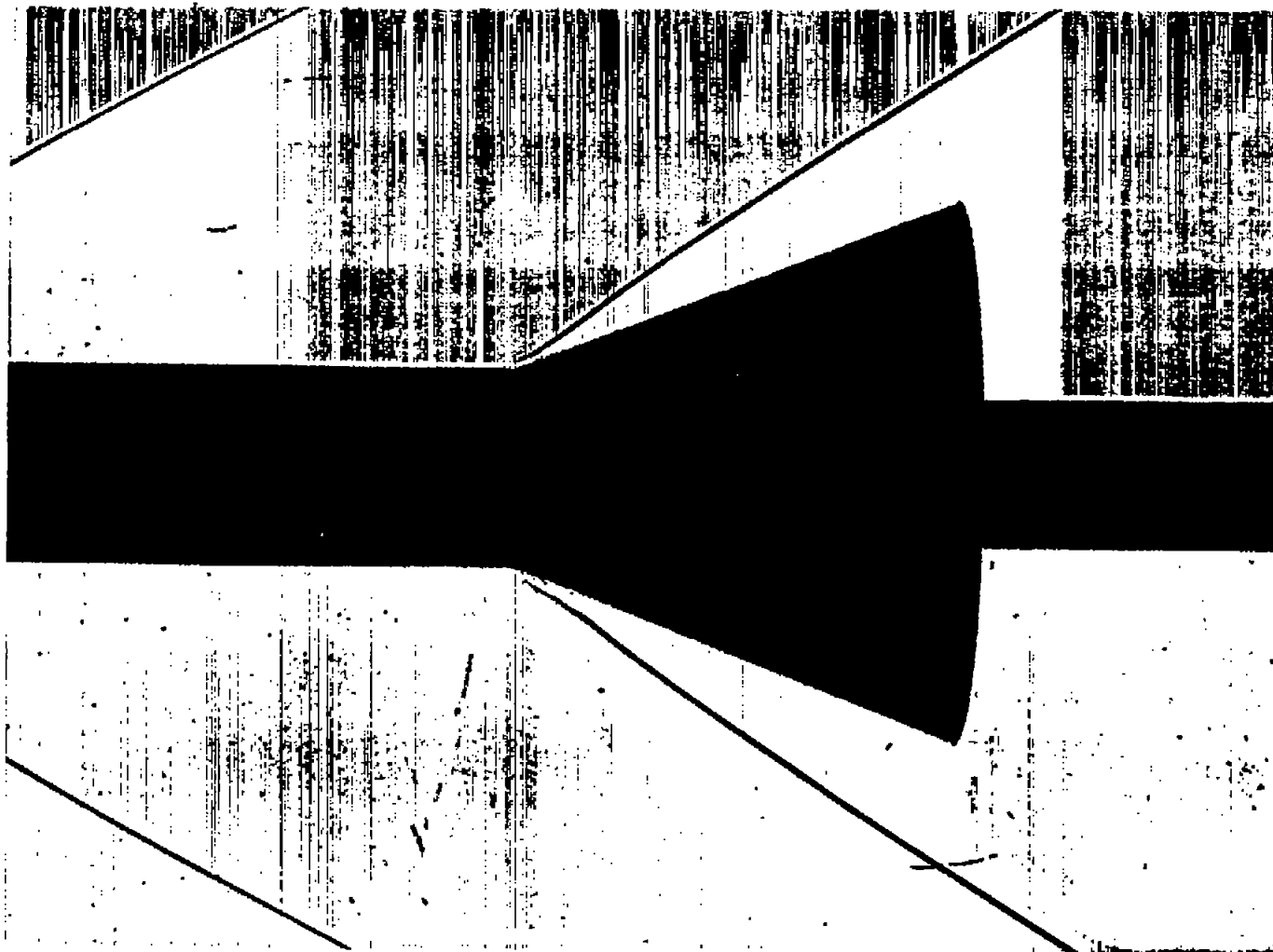
[REDACTED]

[REDACTED]



All dimensions in inches.

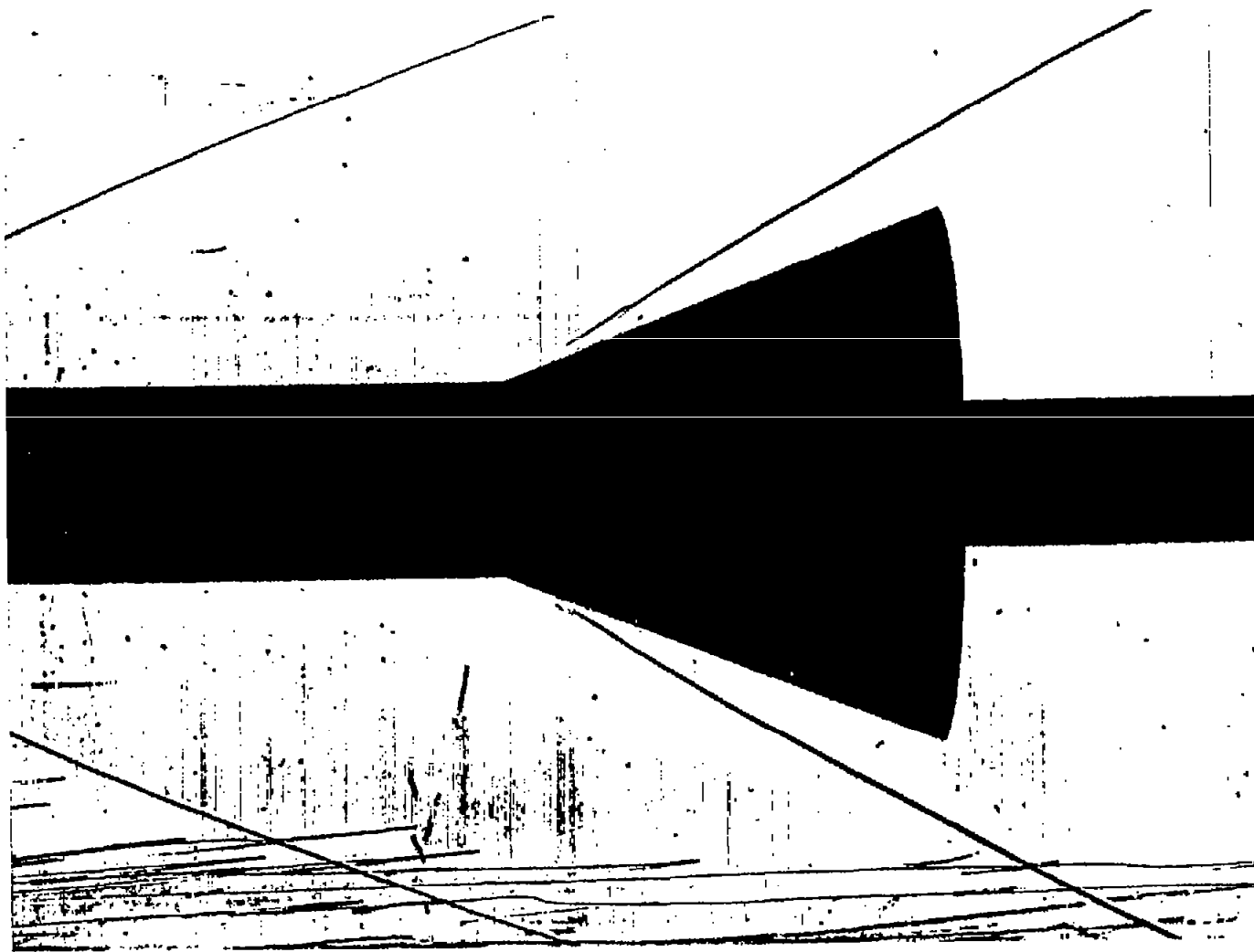
Figure 1.- Cone-cylinder cone-frustum test body.



(a) $M = 3.00$

A-20481

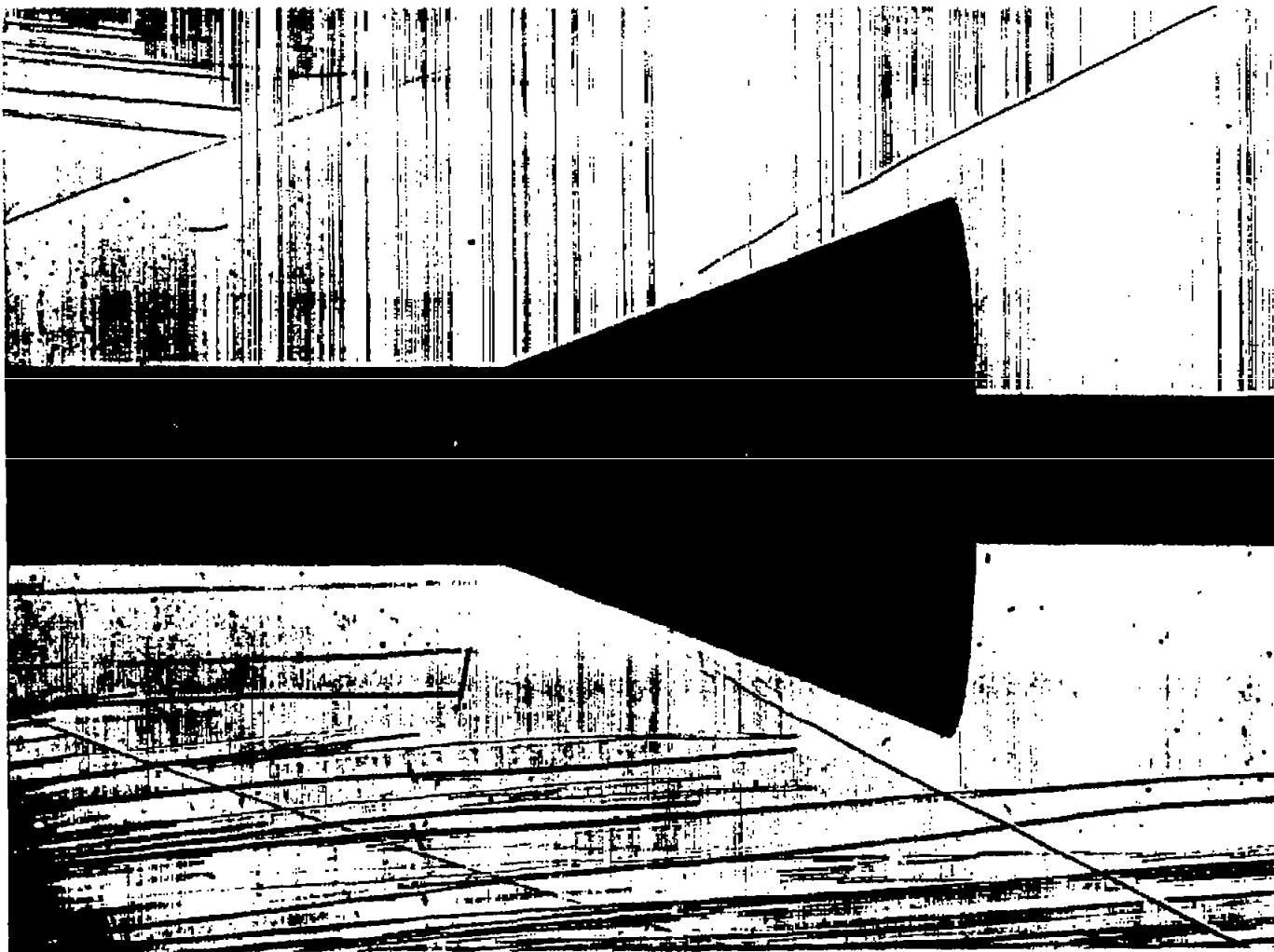
Figure 2.- Shadowgraph pictures of flow in region of cylinder-frustum juncture.



A-30482

(b) $M = 4.24$

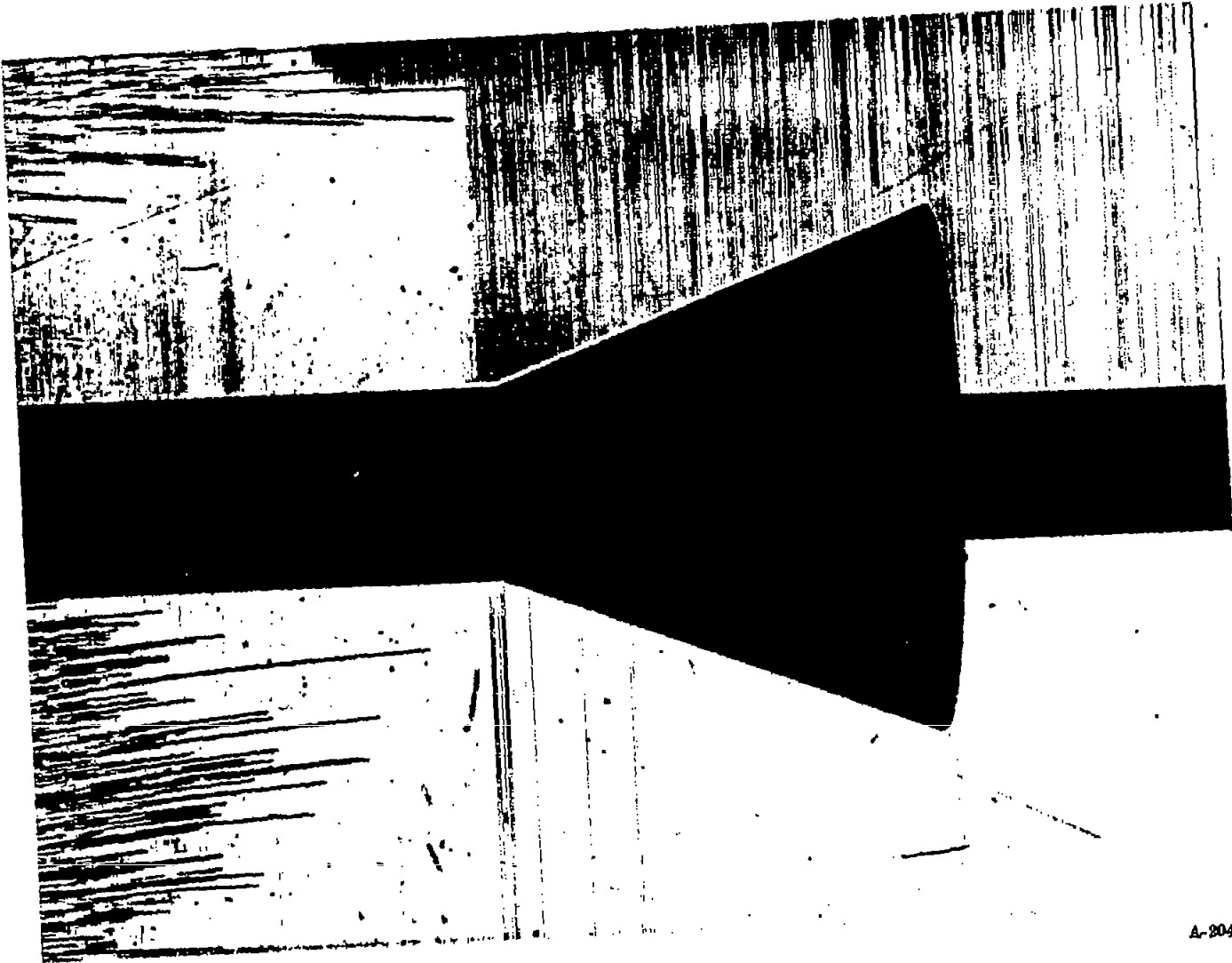
Figure 2.- Continued.



(c) $M = 5.05$

A-20483

Figure 2.- Continued.



(d) $M = 6.28$

Figure 2.- Concluded.

A-20464

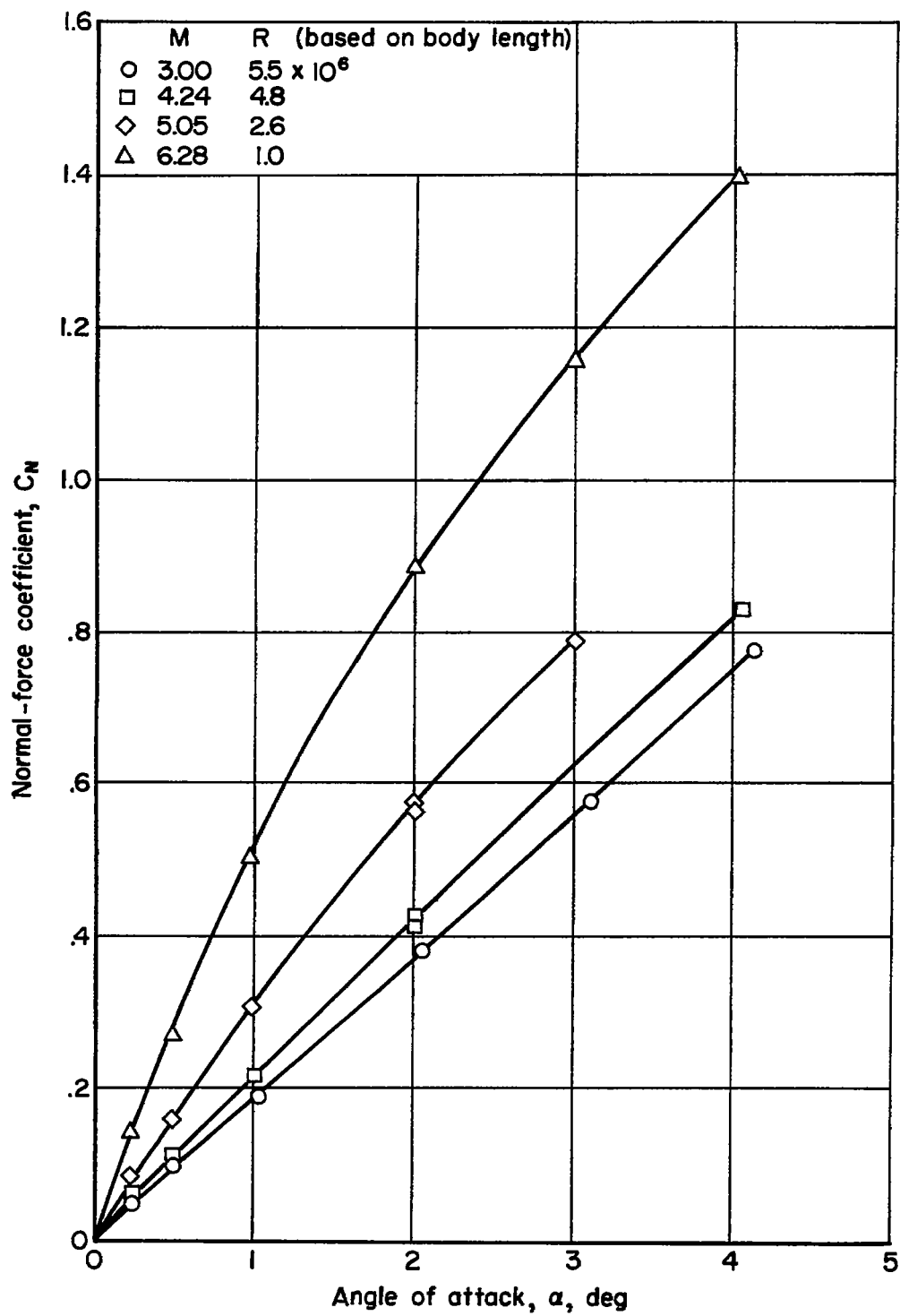


Figure 3.- Normal-force coefficients.

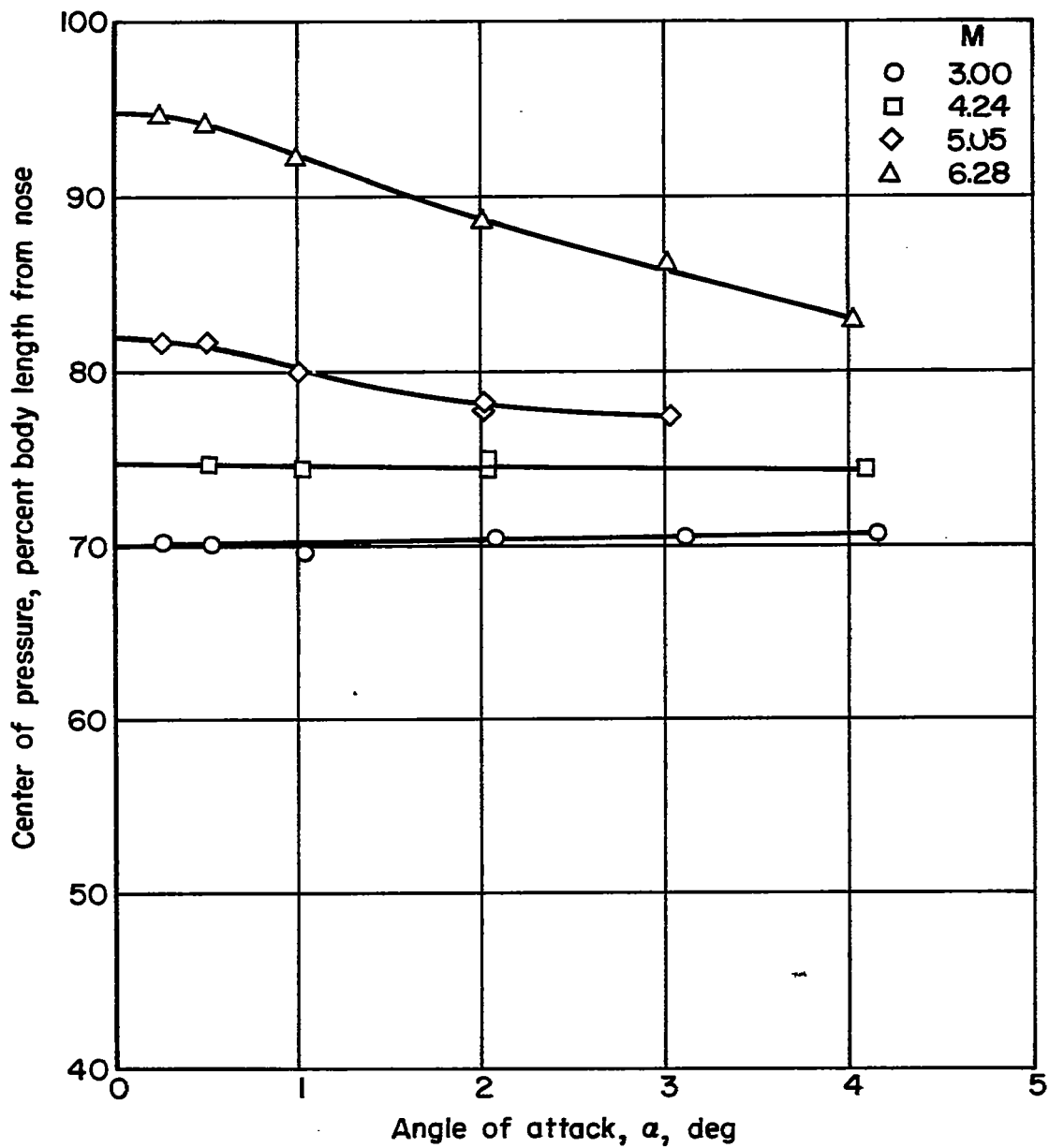


Figure 4.- Center-of-pressure locations.

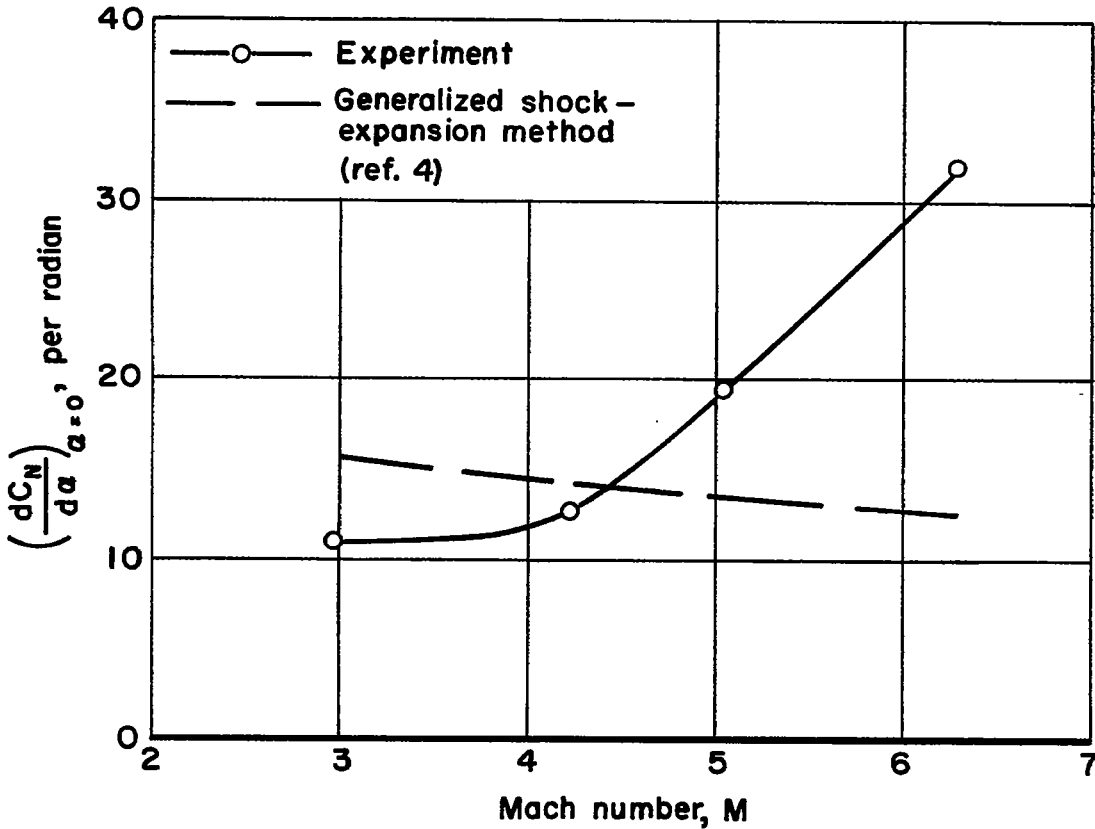
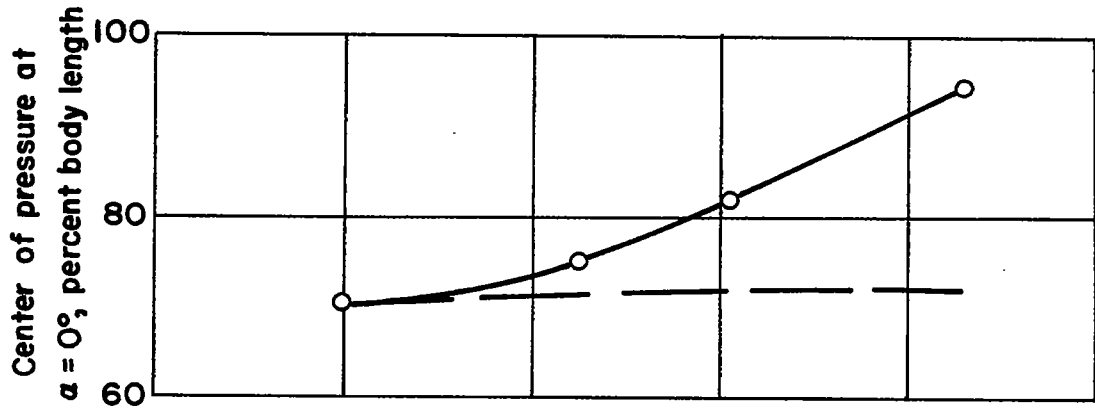


Figure 5.— Normal-force derivatives and center-of-pressure locations at zero angle of attack.